Acta Crystallographica Section C
Crystal Structure Communications
ISSN 0108-2701

The ferriannite $KFe^{2+}_3(Al_{0.26}Fe^{3+}_{0.76}Si_3)O_{10}(OH)_2$ at 100 and 270 K

Günther J. Redhammer* and G. Roth

Institute of Crystallography, RWTH Aachen, Jägerstraße 17/19, D-52056 Aachen, Germany
Correspondence e-mail: guenther.redhammer@aon.at

Received 25 November 2003
Accepted 10 February 2004
Online 11 March 2004

Unusually large and good-quality single crystals of the synthetic trioctahedral mica $KFe^{2+}_3(Al_{0.26}Fe^{3+}_{0.76}Si_3)O_{10}(OH)_2$ [potassium triiron(II) aluminasilaferrate(III) decaoxide dihydroxide] have been grown hydrothermally. X-ray diffraction data measured at 270 and 100 K have been used to refine the crystal structure, including the positions of the H atoms. This synthetic mica is similar to annite, $KFe_3AlSi_3O_{10}(OH)_2$, and crystallizes with the same monoclinic $C2/m$ symmetry. No phase transition has been observed down to 100 K. At low temperature, the ditrigonal distortion of the mica structure increases markedly, while the octahedral and tetrahedral bond lengths tend to decrease and increase, respectively. A detailed comparison of structural parameters in various Fe-rich micas is presented.

Comment

Trioctahedral micas, $XY_3Z_4O_{10}(OH)_2$ (where X is an interlayer cation, Y is an octahedral cation and Z is a tetrahedral cation), are widely occurring rock-forming minerals. Their crystal chemistry is complex as they can accommodate a large variety of cations into their structure. Systematic structural and spectroscopic studies of synthetic micas are thus important in order to obtain a more complete understanding of the crystal chemical variations with changing chemical composition.

Natural trioctahedral micas have been investigated intensively by single-crystal X-ray diffraction methods, and a recent review on mica crystal chemistry is found in Brigatti & Guggenheim (2002). However, studies on Fe-rich micas are rare. The Fe-bearing mica closest to the ideal composition of the mineral annite, $KFe_3AlSi_3O_{10}(OH)_2$, is that studied by Redhammer & Roth (2002), with a composition of $(K_{0.94}Na_{0.07})(Fe^{2+}_{2.25}Fe^{3+}_{0.28}Mn_{0.18}Mg_{0.07}Ti_{0.08})(Al_{0.98}Fe^{3+}_{0.19}Si_{2.83})O_{10}(OH_{1.85}F_{0.15})$. In addition to natural trioctahedral micas, Redhammer & Roth (2002) also studied a variety of synthetic samples with various octahedral contents but containing no tetrahedral ferric iron. Other structural studies of tetraferrimicas have been carried out for $CsFe_3(Fe^{3+}Si_3)O_{10}(OH)_2$ (Mellini *et al.*, 1996; Comodi *et al.*, 1999) and $RbFe_3(Fe^{3+}Si_3)O_{10}(OH)_2$ (Comodi *et al.*, 2003). Donnay *et al.* (1964) were the first workers to refine the structure of a synthetic tetraferriannite (TFA), $KFe_3(Fe^{3+}Si_3)O_{10}(OH)_2$, from film data. However, a complete refinement was not possible and no anisotropic displacement parameters were refined, nor were the H atoms located. To date, no data are available for K-containing trioctahedral micas containing Fe exclusively in the octahedral sheet. In the course of our investigations on micas of the formula $KFe_3(Al_{1-x}Fe^{3+}_xSi_3)O_{10}(OH)_2$, unusually large (about 500 µm long) and good-quality single crystals of the title compound, (I), were obtained: its crystal structures at 100 and 270 K are described here and compared with the structures of the near-end-member annite (Redhammer & Roth, 2002) and Rb and Cs tetraferriannites (Comodi *et al.*, 1999, 2003).

Fig. 1 depicts part of the structure the title compound. Other polyhedral representations of the mica structure may be found in the literature (*e.g.* Brigatti & Guggenheim, 2002). The discussion below refers to the structure at 270 K.

The octahedral sheet of the structure of (I) contains two different $M1$ and $M2$ sites which each carry an OH group. The H atom is located 0.87 (4) Å from atom O4 and the O—H bond is not exactly perpendicular to the (001) plane, but slightly inclined along the a axis towards the centre of the ring defined by six TO_4 tetrahedra (with T = Si^{4+}, Al^{3+}, Fe^{3+}). The average $M1$—O bond in (I) [2.119 (1) Å; Table 2] is similar to that in the end-member tetraferriannite [2.11 (1) Å; Donnay *et al.*, 1964]. The average $M1$—O bond length increases with the size of the interlayer cation (Table 2), as a result of the expansion of the unit cell, not only along [001] (which is most sensitive to changes in the interlayer chemistry), but also within the (001) plane. The bond-length distortion (BLD in Table 2) of the $M1$ octahedron is small and similar to that found for annite and the Rb and Cs tetraferriannites. However, the edge-length ratio (e_u/e_s; Toraya, 1981) and the octahedral-angle variance (OAV; Robinson *et al.*, 1971) both indicate a significant angular distortion of the $M1$ site, as does the octahedral flattening angle (ψ), which is distinctly larger than its ideal value of 54.73°. Replacing K in the interlayer by Rb or Cs increases the octahedral flattening and reduces the thickness of the octahedral sheet (Table 2). The polyhedral distortion of the $M2$ site is similar to that of $M1$. This is a general feature of all trioctahedral micas, except those containing octahedrally coordinated Al^{3+} (Redhammer & Roth, 2002). As observed for $M1$, the average $M2$—O bond length is somewhat larger than in synthetic tetraferriannite (Donnay *et al.*, 1964).

The average T—O bond length in the title compound [1.676 (1) Å] is somewhat shorter than in the Rb or Cs tetraferriannites, or tetraferriphlogopite [1.680 (2) Å; Brigatti *et al.*, 1996]. This is related to the presence of tetrahedral Al^{3+} in addition to Si^{4+} and Fe^{3+}. It has been noted by Brigatti *et al.* (1996) that the substitution of tetrahedral Al^{3+} by larger cations, such as Fe^{3+}, produces more regular tetrahedra. This effect is also observed here, as shown by the smaller BLD and

 DOI: 10.1107/S010827010400321X

tetrahedral angle variance (TAV) (Table 2). As a result of the Fe^{3+}/Al^{3+} tetrahedral substitution, the dimensional misfit between the octahedral and tetrahedral sheets increases but is compensated for by an increase of the tetrahedral ring-distortion angle (α in Table 2). This distortion of the tetrahedral sheet directly influences the coordination geometry of the interlayer cation. Whereas the inner and outer K—O bond lengths are similar when the ditrigonal distortion is small (*e.g.* near-end-member annites, Rb-TFA and Cs-TFA), the difference between the K—O distances increases with increasing tetrahedral rotation, α (Table 2). Due to the expansion of the octahedral sheet in the (001) plane of Rb- and Cs-TFA, the tetrahedral ring has a nearly ideal hexagonal geometry in these structures.

At room temperature, the lattice parameters of (I) are larger than those of pure annite (*e.g.* Redhammer *et al.*, 1993; Redahmmer & Roth, 2002) but slightly smaller than those of pure tetraferriannite [a = 5.4354 (6) Å, b = 9.4186 (7) Å, c = 10.3449 (5) Å and β = 100.121 (14)°; Redhammer *et al.*, 2004]. These differences are attributed to the different composition of the tetrahedral sheet. Upon cooling from 270 to 100 K, the lattice parameters decrease significantly and yield linear thermal expansion coefficients of 11.1×10^{-6}, 10.8×10^{-6} and 21.6×10^{-6} K^{-1} for the a, b and c axes, respectively. These coefficients are similar to those in near-end-member phlogopite, *viz*. 8.6, 7.5 and 18.1 (all $\times$ 10^{-6} K^{-1}; Russell & Guggenheim, 1999). The thermal expansion along **c** is twice as large as that within the (001) plane. The [001] direction corresponds to the stacking of the negatively charged 2:1 layers and is the direction most affected by the thermal motion of the interlayer K^+ cation.

In addition to the shortening of the unit-cell parameters, the most pronounced changes upon cooling from 270 to 100 K are observed for the interlayer region of the structure. The average $K—O_{inner}$ bond shortens, while the average $K—O_{outer}$ bond lengthens, corresponding to an increase of the ditrigonal distortion (Table 2). This increase, as measured by a larger rotation angle α, is related to the different thermal expansion of the octahedral and tetrahedral sheets, whereby the average

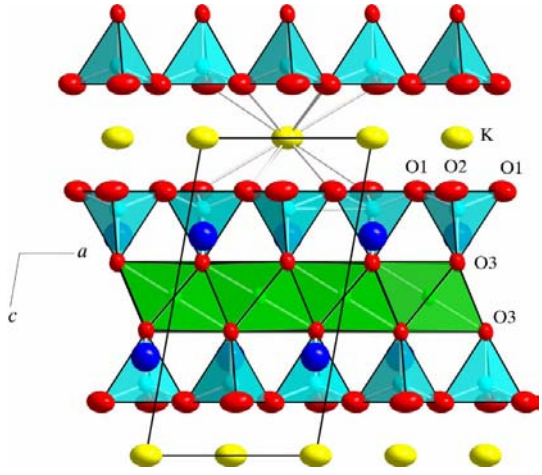

Figure 2
Polyhedral representation of the structure of $KFe_3(Al_{0.24}Fe^{3+}_{0.76})Si_3O_{10}(OH)_2$ at 270 K in a projection along the b axis, showing the 2:1 layer and its interconnection by the interlayer cations.

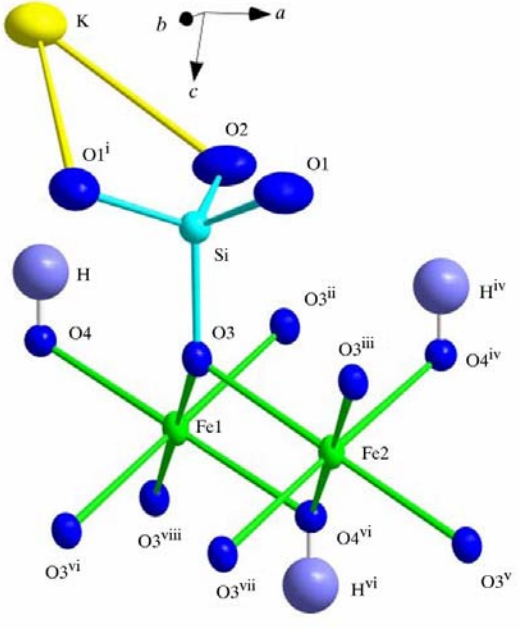

Figure 1
Part of the $KFe_3(Al_{0.24}Fe^{3+}_{0.76})Si_3O_{10}(OH)_2$ structure at 270 K, with displacement ellipsoids drawn at the 90% probability level. [Symmetry codes: (i) $x-\frac{1}{2}, \frac{1}{2}-y, z$; (ii) $x, -y, z$; (iii) $\frac{1}{2}+x, \frac{1}{2}-y, z$; (iv) $1+x, y, z$; (v) $2-x, y, 1-z$; (vi) $1-x, y, 1-z$; (vii) $\frac{3}{2}-x, \frac{1}{2}-y, 1-z$; (viii) $1-x, -y, 1-z$.]

M—O bond lengths tend to decrease at low temperature while the average T—O bond lengths tend to increase (Table 2). Although the changes in bond length (0.003 Å) are only slightly larger than the standard uncertainty (0.001 Å), an equivalent trend was observed for a near-end-member phlogopite, $KMg_3AlSi_3O_{10}(OH)_2$, in which the average T—O bond length decreased by 0.004 Å upon heating from 293 to 873 K (Russell & Guggenheim, 1999). The decrease in the tetrahedral angle τ upon cooling (Table 2) indicates that the tetrahedra are slightly elongated along the c axis at high temperature and compressed at low temperature.

The anisotropic atomic displacement parameters (ADPs) are also affected by cooling. Atoms O1 and O2, which are shared between tetrahedra, show larger ADPs than atoms O3 and O4, which bridge tetrahedra and octahedra (Fig. 1). This suggests that the latter are more rigidly bonded than the former. The interlayer K^+ cation shows a more anisotropic displacement than the octahedral cations, while the displacement of the tetrahedral cation is nearly isotropic. This behaviour is generally observed in all trioctahedral micas. Upon cooling to 100 K, the displacement decreases by ~47% for the K site, ~38% for the M sites, 26% for the T site and 30% for the O sites. Only minor changes are observed in the ADP max/min ratios, indicating that there is no significant change in the anisotropic behaviour of the atoms.

Experimental

Single crystals of the title compound were synthesized under hydrothermal conditions using temperature-gradient experiments in 5 cm long Au tubes at 973 K under a hydrostatic pressure of 0.4 GPa. Stoichiometric amounts of K_2CO_3, Fe_2O_3, Al_2O_3 and SiO_2 were carefully ground to a homogeneous fine-grained powder in an agate mortar under alcohol. This powder was the starting material for the synthesis. The oxygen fugacity during the experiment was determined by the high-pressure vessel and was close to the nickel/nickel-oxide solid-state buffer. A small number of unusually large mica single crystals with a nearly prismatic habit formed at the 'cold' end of the Au capsule. This crystal shape is unusual, as micas normally form thin flakes.

Ferriannite (I) at 270 K

Crystal data

$KFe_3(Al_{0.26}Fe_{0.76}Si_3)O_{10}(OH)_2$
M_r = 533.82
Monoclinic, $C2/m$
a = 5.4208 (14) Å
b = 9.3881 (17) Å
c = 10.330 (3) Å
β = 100.06 (2)°
V = 517.6 (2) Å^3
Z = 2
D_x = 3.425 Mg m^{-3}
Mo $K\alpha$ radiation
Cell parameters from 3729 reflections
θ = 2.1–32.3°
μ = 6.00 mm^{-1}
T = 270 (1) K
Cuboid, dark brown
0.17 × 0.14 × 0.10 mm

Data collection

Stoe IPDS-2 diffractometer
Rotation scans
Absorption correction: numerical *via* equivalents (*X-SHAPE* and *X-RED*; Stoe & Cie, 1996)
T_{min} = 0.36, T_{max} = 0.52
3927 measured reflections
938 independent reflections
814 reflections with $I > 2\sigma(I)$
R_{int} = 0.027
θ_{max} = 32.1°
$h = -7 \rightarrow 8$
$k = -11 \rightarrow 14$
$l = -15 \rightarrow 15$

Refinement

Refinement on F^2
$R(F)$ = 0.020
$wR(F^2)$ = 0.049
S = 1.10
938 reflections
59 parameters
All H-atom parameters refined
$w = 1/[\sigma^2(F_o^2) + (0.0278P)^2]$ where $P = (F_o^2 + 2F_c^2)/3$
$(\Delta/\sigma)_{max}$ = 0.001
$\Delta\rho_{max}$ = 0.40 e Å^{-3}
$\Delta\rho_{min}$ = −0.50 e Å^{-3}
Extinction correction: *SHELXL*97 (Sheldrick, 1997)
Extinction coefficient: 0.0147 (8)

Table 1
Selected geometric parameters (Å, °) for (I) at 270 K.

Fe1—O4	2.1004 (14)	Si—O1	1.6759 (13)
Fe1—O3^{i}	2.1277 (9)	Si—O1^{iii}	1.6765 (13)
Fe2—O4^{i}	2.1037 (9)	K—O2	3.050 (2)
Fe2—O3^{ii}	2.1195 (10)	K—O1^{iv}	3.0513 (14)
Fe2—O3	2.1301 (11)	K—O2^{iv}	3.364 (2)
Si—O2	1.6758 (7)	K—O1^{iii}	3.3637 (15)
Si—O3	1.6758 (11)		
O4^{i}—Fe1—O3^{v}	95.65 (4)	O4^{vi}—Fe2—O3	95.16 (4)
O4—Fe1—O3^{v}	84.35 (4)	O3^{vii}—Fe2—O3^{viii}	94.92 (4)
O3^{v}—Fe1—O3^{i}	94.56 (5)	O2—Si—O3	109.94 (6)
O3^{v}—Fe1—O3	85.44 (5)	O2—Si—O1	109.05 (8)
O4^{i}—Fe2—O4^{vi}	82.73 (5)	O3—Si—O1	109.94 (6)
O4^{i}—Fe2—O3^{vii}	95.72 (4)	O2—Si—O1^{iii}	108.98 (8)
O3^{vii}—Fe2—O3^{ii}	85.85 (5)	O3—Si—O1^{iii}	109.91 (5)
O3^{ii}—Fe2—O3^{viii}	85.70 (4)	O1—Si—O1^{iii}	109.00 (4)
O4^{vi}—Fe2—O3^{viii}	84.21 (4)		

Symmetry codes: (i) $1-x, -y, 1-z$; (ii) $\frac{1}{2}+x, \frac{1}{2}-y, z$; (iii) $x-\frac{1}{2}, \frac{1}{2}-y, z$; (iv) $x-1, y, z$; (v) $1-x, y, 1-z$; (vi) $1+x, y, z$; (vii) $\frac{3}{2}-x, \frac{1}{2}-y, 1-z$; (viii) $2-x, y, 1-z$.

Ferriannite (I) at 100 K

Crystal data

$KFe_3(Al_{0.26}Fe_{0.76}Si_3)O_{10}(OH)_2$
M_r = 533.82
Monoclinic, $C2/m$
a = 5.4106 (13) Å
b = 9.3709 (16) Å
c = 10.293 (3) Å
β = 100.03 (2)°
V = 513.9 (2) Å^3
Z = 2
D_x = 3.453 Mg m^{-3}
Mo $K\alpha$ radiation
Cell parameters from 4863 reflections
θ = 2.1–32.3°
μ = 6.07 mm^{-1}
T = 100 (1) K
Cuboid, dark brown
0.17 × 0.14 × 0.10 mm

Data collection

Stoe IPDS-2 diffractometer
Rotation scans
Absorption correction: numerical *via* equivalents (*X-SHAPE* and *X-RED*; Stoe & Cie, 1996)
T_{min} = 0.36, T_{max} = 0.52
4927 measured reflections
934 independent reflections
825 reflections with $I > 2\sigma(I)$
R_{int} = 0.028
θ_{max} = 32.1°
$h = -8 \rightarrow 8$
$k = -11 \rightarrow 14$
$l = -15 \rightarrow 15$

Refinement

Refinement on F^2
$R(F)$ = 0.019
$wR(F^2)$ = 0.052
S = 1.09
934 reflections
59 parameters
All H-atom parameters refined
$w = 1/[\sigma^2(F_o^2) + (0.0298P)^2 + 0.3868P]$ where $P = (F_o^2 + 2F_c^2)/3$
$(\Delta/\sigma)_{max} < 0.001$
$\Delta\rho_{max}$ = 0.42 e Å^{-3}
$\Delta\rho_{min}$ = −0.42 e Å^{-3}
Extinction correction: *SHELXL*97 (Sheldrick, 1997)
Extinction coefficient: 0.0090 (8)

Table 2
Selected geometric parameters (Å, °) for (I) at 100 K.

Fe1—O4	2.0990 (15)	Si—O2	1.6792 (8)
Fe1—O3	2.1245 (10)	Si—O1^{iii}	1.6811 (14)
Fe2—O4^{i}	2.1003 (9)	K—O1^{iv}	2.9894 (15)
Fe2—O3^{ii}	2.1174 (10)	K—O2	2.993 (2)
Fe2—O3	2.1266 (12)	K—O2^{iv}	3.401 (2)
Si—O3	1.6751 (12)	K—O1^{iii}	3.4045 (16)
Si—O1	1.6790 (14)		
O4—Fe1—O3^{v}	95.60 (4)	O3^{viii}—Fe2—O3	85.73 (4)
O4^{vi}—Fe1—O3^{v}	84.40 (4)	O3^{ii}—Fe2—O3	94.86 (4)
O3^{v}—Fe1—O3	94.50 (6)	O3—Si—O1	109.72 (6)
O3^{vii}—Fe1—O3	85.50 (6)	O3—Si—O2	109.76 (7)
O4^{i}—Fe2—O4^{vi}	82.84 (6)	O1—Si—O2	109.17 (8)
O4^{vi}—Fe2—O3^{viii}	95.66 (4)	O3—Si—O1^{iii}	109.82 (6)
O3^{ii}—Fe2—O3^{viii}	85.85 (6)	O1—Si—O1^{iii}	109.16 (5)
O4^{vi}—Fe2—O3	84.32 (5)	O2—Si—O1^{iii}	109.19 (8)
O4^{i}—Fe2—O3	95.07 (5)		

Symmetry codes: (i) $1+x, y, z$; (ii) $\frac{1}{2}+x, \frac{1}{2}-y, z$; (iii) $x-\frac{1}{2}, \frac{1}{2}-y, z$; (iv) $1-x, -y, -z$; (v) $x, -y, z$; (vi) $1-x, -y, 1-z$; (vii) $1-x, y, 1-z$; (viii) $\frac{3}{2}-x, \frac{1}{2}-y, 1-z$.

Several crystals were examined before the full data collection was carried out. Analysis of the systematic absences confirmed the *C*-centred space group, identifying the polytype as 1*M*. The composition of the tetrahedral site was determined by assuming an ideal Si content (0.75) and refining variable amounts of Al^{3+} (x) and Fe^{3+} ($\frac{1}{4}-x$). The refined composition is close to that determined by microprobe analysis of fine-grained mica products of the same experiment (Redhammer *et al.*, 2004). Mellini *et al.* (1996) noted residual electron-density maxima located at *b*/3 from the original atom positions and interpreted them as due to faults in the stacking sequence along the [001] direction. No significant residual electron

Table 3
Structural parameters for selected Fe-bearing trioctahedral 1*M* micas.

Bond-length distortion (BLD) = $(100/n)\sum_{i=1}^{n}\{[(X-O)_i - (<X-O>)]/(<X-O>)\}$, with n = number of bonds, $(X-O)_i$ = central cation-to-oxygen length and <*X*—O> = average cation–oxygen bond length (Renner & Lehmann, 1986); edge-length distortion (ELD) = $(100/n)\sum_{i=1}^{n}\{[(O-O)_i - (<O-O>)]/(<O-O>)\}$, with n = number of edges, $(O-O)_i$ = polyhedron edge length and <O—O> = average polyhedron edge length (Renner & Lehmann, 1986); octahedral angle variance (OAV) = $\sum_{i=1}^{n}(\theta_i - 90)^2/11$ (Robinson *et al.*, 1971); octahedral flattening angle ψ: $\cos\psi = t_{oct}/2d_{oct}$, with d_{oct} = average *M*—O distance and t_{oct} = octahedral sheet thickness, $t_{oct} = 2\{\frac{1}{2} - [2(z_{O3} - z_{O4})/3]\}c\sin\beta$; unshared edge e_u/shared edge e_s (Toraya, 1981); tetrahedral angle variance (TAV) = $\sum_{i=1}^{n}(\theta_i - 109.47)^2/5$ (Robinson *et al.*, 1971); τ = mean of the three $O_{basal}-T-O_{apex}$ angles; α = ditrigonal distortion of the tetrahedral sheet with $\tan\alpha = 4 \times 3^{\frac{1}{2}}(\frac{1}{4} - y_{O1})$.

Sample	Annite†	TFA-1‡	TFA-2§	Rb-TFA¶	Cs-TFA††
*M*1 site:					
Volume (Å^3)	12.63 (3)	12.50 (2)	12.46 (2)	12.56 (6)	12.67 (5)
BLD (°)	0.21	0.57	0.53	0.52	0.46
ELD (°)	4.17	4.58	4.52	5.14	5.33
OAV (°)	26.37	30.81	30.16	41.71	42.27
ψ (°)	58.28	58.57	58.53	59.23	59.29
e_u/e_s	1.089	1.097	1.096	1.109	1.114
<*M*1—O> (Å)	2.129 (1)	2.119 (1)	2.116 (1)	2.126 (4)	2.134 (5)
*M*2 site:					
Volume (Å^3)	12.56 (3)	12.49 (2)	12.44 (2)	12.56 (3)	12.61 (9)
BLD (°)	0.38	0.44	0.46	0.41	0.55
ELD (°)	4.03	4.44	4.38	5.24	5.17
OAV (°)	25.52	31.01	30.21	42.12	41.54
ψ (°)	58.20	58.55	58.51	59.23	59.19
e_u/e_s	1.087	1.096	1.095	1.114	1.113
t_{oct} (Å)	2.238	2.210	2.210	2.175	2.180
<*M*2—O> (Å)	2.124 (1)	2.118 (1)	2.115	2.126 (4)	2.128 (5)
T site:					
Volume (Å^3)	2.36 (1)	2.42 (1)	2.43 (1)	2.46 (1)	2.47 (2)
BLD (°)	0.14	0.02	0.10	0.23	0.28
TAV (°)	0.83	0.26	0.11	0.34	1.44
<*T*—O> (Å)	1.668 (1)	1.676 (1)	1.679 (1)	1.687 (4)	1.688 (4)
τ (°)	110.29	109.62	109.17	110.00	110.52
α (°)	2.48	6.74	8.90	2.26	0.16
Interlayer site:					
$K-O_{inner}$ (Å)	3.138 (1)	3.051 (2)	2.991 (2)	3.227 (6)	3.359 (6)
$K-O_{outer}$ (Å)	3.255 (1)	3.364 (2)	3.403 (2)	3.330 (5)	3.372 (6)
$\Delta_{(outer-inner)}$	0.133	0.313	0.412	0.103	0.013

† Natural annite (Redhammer & Roth, 2002). ‡ Tetraferriannite at 270 K (this work). § Tetraferriannite at 100 K (this work). ¶ Rb tetraferriannite (Comodi *et al.*, 2003). †† Cs tetraferriannite (Comodi *et al.*, 1999).

density was observed in the case of the present crystals, including those with a large dimension along *c*. Structure refinements carried out on two additional crystals from the same synthesis batch yielded identical results to those presented here, within one standard uncertainty.

For compound (I) at both temperatures, data collection: *X-AREA* (Stoe & Cie, 2002); cell refinement: *X-AREA*; data reduction: *X-AREA*; program(s) used to solve structure: *SHELXS*97 (Sheldrick, 1997); program(s) used to refine structure: *SHELXL*97 (Sheldrick, 1997); molecular graphics: *DIAMOND* (Brandenburg & Berndt, 1999); software used to prepare material for publication: *WinGX* (Farrugia, 1999).

GJR thanks the Austrian Academy of Science for financial support *via* an APART (Austrian Programme for Advanced Research and Technology) scholarship during 2000–2003, and the Austrian Science Foundation (FWF) for financial support through grant No. R33-N10. The thorough review of an anonymous referee and the kind help of Jacques Barbier in improving the impact of the paper are greatly acknowledged.

Supplementary data for this paper are available from the IUCr electronic archives (Reference: BC1034). Services for accessing these data are described at the back of the journal.

References

Brandenburg, K. & Berndt, M. (1999). *DIAMOND*. Release 2.1b. Crystal Impact GbR, Bonn, Germany.
Brigatti, M. F. & Guggenheim, S. (2002). *Rev. Miner. Geochem.* **46**, 1–97.
Brigatti, M. F., Medici, L. & Poppi, L. (1996). *Clays Clay Miner.* **44**, 540–545.
Comodi, P., Drabek, M., Montagnoli, M., Rieder, M., Weiss, Z. & Zanazzi, P. F. (2003). *Phys. Chem. Miner.* **30**, 198–205.
Comodi, P., Zanazzi, P. F., Weiss, Z., Rieder, M. & Drabeck, M. (1999). *Am. Miner.* **84**, 325–332.
Donnay, G., Morimoto, N., Takeda, H. & Donnay, J. D. H. (1964). *Acta Cryst.* **17**, 1369–1373.
Farrugia, L. J. (1999). *J. Appl. Cryst.* **32**, 837–838.
Mellini, M., Weiss, Z., Rieder, M. & Drabeck, M. (1996). *Eur. J. Miner.* **8**, 1265–1271.
Redhammer, G. J., Amthauer, G., Lottermoser, W., Bernroider, M., Tippelt, G. & Roth, G. (2004). In preparation.
Redhammer, G. J., Beran, A., Dachs, E. & Amthauer, G. (1993). *Phys. Chem. Miner.* **20**, 382–394.
Redhammer, G. J. & Roth, G. (2002). *Am. Miner.* **87**, 1464–1476.
Renner, B. & Lehmann, G. (1986). *Z. Kristallogr.* **175**, 43–59.
Robinson, K., Gibbs, G. V. & Ribbe, P. H. (1971). *Science*, **172**, 567–570.
Russell, R. L. & Guggenheim, S. (1999). *Can. Miner.* **37**, 711–720.
Sheldrick, G. M. (1997). *SHELXS*97 and *SHELXL*97. University of Göttingen, Germany.
Stoe & Cie (1996). *X-SHAPE* and *X-RED*. Stoe & Cie, Darmstadt, Germany.
Stoe & Cie (2002). *X-AREA*. Stoe & Cie, Darmstadt, Germany.
Toraya, H. (1981). *Z. Kristallogr.* **157**, 173–190.